UDC 621.3 https://doi.org/10.20998/2074-272X.2024.6.05

A. Zorig, N. Hamouda, B. Babes, S. Mouassa

Improving the efficiency of a non-ideal grid coupled to a photovoltaic system with a shunt active power filter using a self-tuning filter and a predictive current controller

Introduction. *Recently, photovoltaic (PV) systems are increasingly favored for converting solar energy into electricity. PV power systems have successfully evolved from small, standalone installations to large-scale, grid-connected systems. When the nonlinear loads are connected to a grid-tied PV system, the power quality can deteriorate due to the active power supplied by the PV array, there's a noticeable decline in the quality of power delivered to consumers. Its combination with the shunt active power filter (SAPF) enhances system efficiency. Consequently, this integrated system is adept at not only powering local loads but also at compensating for reactive power and filtering out harmonic currents from the main grid. The* ***novelty*** *of the work describes how an operation of a small scale PV system connected to the low voltage distribution system, and nonlinear load can be achieved, the investigation aims to analyze the system's behavior and elucidate the advantages of employing various control algorithms. These proposed algorithms are designed to ensure a unity power factor for the utility grid while prioritizing high convergence speed and robustness against load power fluctuations across different levels of solar irradiation affecting the PV modules. The* ***purpose*** *of this work is to enhance the dynamic performance of the SAPF by cooperatively using a self-tuning filter (STF) based instantaneous active and reactive power method (PQ) with a novel predictive current control, enhance the system resilience, ensure optimal management of the total active power between the PV system, the electrical network and the non-linear load by integrating the functionalities of the SAPF under different levels of solar irradiation and maintain the DC-link capacitor voltage constant.* ***Methods****. A novel predictive current controller is designed to generate the switching signals piloted the three phase source voltage inverter, also a novel algorithm of instantaneous active and reactive power is developed, based on STF, to extract accurately the harmonic reference under non ideal grid voltage, also the perturb and observe algorithm is used to extract, under step change of solar irradiation, the maximum power point tracking of the PV module and the PI controller is used to maintain constant the DC-link capacitor voltage of the SAPF.* ***Results.*** *The efficacy of the proposed system is primarily centered on the grid side, and the performance evaluation of the control system is conducted using the STF based PQ algorithm and predictive current control. In addition, comprehensive testing encompasses all modes of operation, including scenarios involving distorted voltage sources, step changes in solar radiation, and variations in nonlinear loads. Results highlight superior performance in both transient and stable states, affirming the robustness and effectiveness of the proposed controllers.* ***Practical value****. The total harmonic distortion value of the grid current for all tests respects the IEEE Standard 519-1992.* References 21, tables 7, figures 25.

Key words: **photovoltaic system, shunt active power filter, active and reactive power algorithm, self-tuning filter, total harmonic distortion, predictive current control, maximum power point tracking.**

Вступ*. Останнім часом фотоелектричні (PV) системи все частіше використовуються для перетворення сонячної енергії на електрику. Фотоелектричні системи успішно еволюціонували від невеликих автономних установок до великомасштабних систем, підключених до мережі. Коли нелінійні навантаження підключені до мережевої фотоелектричної системи, якість електроенергії може погіршитися через активну потужність фотоелектричної матриці, що подається, спостерігається помітне зниження якості електроенергії, що постачається споживачам. Його поєднання із шунтуючим активним фільтром потужності (SAPF) підвищує ефективність системи. Отже, ця інтегрована система здатна як живити локальні навантаження, так і компенсувати реактивну потужність і відфільтровувати гармонійні струми з основний мережі.* ***Новизна*** *роботи описує, як можна домогтися роботи маломасштабної фотоелектричної системи, підключеної до розподільчої системи низької напруги та нелінійного навантаження, дослідження спрямоване на аналіз поведінки системи та з'ясування переваг використання різних алгоритмів управління. Ці алгоритми розроблені для забезпечення одиничного коефіцієнта потужності для комунальної мережі, при цьому віддаючи пріоритет високої швидкості конвергенції та стійкості до коливань потужності навантаження на різних рівнях сонячного опромінення, що впливає на фотоелектричні модулі.* ***Метою*** *даної роботи є підвищення динамічних характеристик SAPF шляхом спільного використання фільтра, що самоналаштовується (STF), на основі методу миттєвої активної та реактивної потужності (PQ) з новим предиктивним управлінням струмом, підвищення стійкості системи, забезпечення оптимального управління загальною активною потужністю між фотоелектричною системою, електричною мережею та нелінійним навантаженням шляхом інтеграції функцій SAPF при різних рівнях сонячного опромінення та підтримання постійної напруги конденсатора ланки постійного струму.* ***Методи****. Новий предиктивний контролер струму, призначений для генерації сигналів перемикання, пілотованих трифазним інвертором напруги джерела, також розроблений новий алгоритм миттєвої активної та реактивної потужності, заснований на самонастроюючому фільтрі, для точного вилучення гармонійного опорного значення при неідеальній напрузі мережі, також використовується алгоритм обурення та спостереження при ступінчастій зміні сонячного випромінювання, відстеження максимальної точки потужності фотоелектричного модуля, а ПІ-регулятор використовується для підтримки постійної напруги конденсатора постійного струму SAPF.* ***Результати****. Ефективність пропонованої системи в першу чергу зосереджена на стороні мережі, а оцінка продуктивності системи керування проводиться з використанням алгоритму PQ на основі STF та керування струмом. Крім того, комплексне тестування охоплює всі режими роботи, включаючи сценарії, що включають спотворені джерела напруги, ступінчасті зміни сонячного випромінювання та зміни нелінійних навантажень. Результати підкреслюють чудову продуктивність як у перехідних, так і у стабільних станах, підтверджуючи надійність і ефективність пропонованих контролерів.* ***Практична цінність****. Загальне значення гармонійних спотворень мережі для всіх випробувань відповідає стандарту IEEE 519-1992.* Бібл. 21, табл. 7, рис. 25.

Ключові слова: **фотоелектрична система, шунтуючий фільтр активної потужності, алгоритм активної та реактивної потужності, фільтр, що самоналаштовується, повне гармонічне спотворення, предиктивне управління струмом, відстеження точки максимальної потужності.**

Introduction. The increasing use of semiconductor devices and nonlinear loads (NLs) in industrial, residential, and commercial sectors has resulted in the degradation of power grid voltage and current waveforms. This, in turn, leads to harmonic distortion in the electrical system [1]. Such harmonics in the power network can cause significant issues including increased power losses, overloading of transmission lines, diminished power quality, reduced equipment efficiency, and disruptions in

device performance. Today, NLs are prevalent in both residential and office spaces [2].

Photovoltaic (PV) systems are increasingly favored for converting solar energy into electricity. In recent times, PV power systems have successfully evolved from small, standalone installations to large-scale, grid-connected systems. When the NLs are connected to a grid-tied PV system, the power quality can deteriorate due to the active power supplied by the PV array. As the adoption of NLs increases, there is a noticeable decline in the quality of power delivered to consumers [3–6]. The shunt active power filter (SAPF) emerges as an adaptable remedy for harmonic compensation. It operates by connecting parallel to the grid and consistently injecting currents that, at any given time, match the harmonic components caused by the NL. The sole use of SAPF is less attractive in practice due to the still high effort involved, especially for powerful systems to be filtered. Hence we are much more interested in filtering system coupled with PV system to ensure several advantages. Integrating a PV system into the grid to benefits local load supply, and its combination with the SAPF enhances system efficiency. Consequently, this integrated system is adept at not only powering local loads, but also at compensating for reactive power and filtering out harmonic currents from the main grid. This ensures that the grid current maintains a sinusoidal waveform and upholds a unity power factor (PF) [7–9].

The first task is to extract the power from the PV generator under varying weather conditions. Hence, employing maximum power point tracking (MPPT) method known perturb and observe (P&O), to maximize energy harvest from a PV generator across diverse radiation levels [10–12]. Then his control is integrated at the DC bus control level of the SAPF, which can be provide the power via an appropriate control of SAPF to fed the NL.

The effectiveness of the SAPF is judged by the shape of the signal which must be the inverted image of the harmonics to be compensated, contained in the load. Then the detection method of reference harmonics plays a role in active filtering because the detected signal presents a reference quantity for controlling the voltage source inverter (VSI) of the SAPF. Many algorithms have been used to generate these harmonics reference [1, 13, 14] and the most used is the instantaneous active and reactive power (PQ) algorithm, the primary algorithm on the grid side is dedicated to determining the optimal reference filter currents crucial for the proficient governance of the SAPF. And advanced approach leverages a self-tuning filter (STF), designed specifically to navigate the control intricacies of the SAPF when faced with voltage distortions [9], the major positive behavior of the STF lies in extracting the fundamental components of the voltage, which also facilitates the computation of an accurate harmonic reference current for scenarios involving non-ideal grid voltage, and fluctuating load conditions [15]. This, in turn, aids in producing compensator currents, achieved through the amalgamation of predictive current control (PCC) and supplementary algorithms [16–19].

The secondary controller utilizes a PI controller for ensuring the DC link voltage remains consistent around its predetermined reference value, especially during sudden load shifts or alterations in solar irradiation, and its capability of has been investigated across all operational modes of the proposed system. Other hand, a novel control current loop applied of SAPF in order to generate the filter currents by thanks the PCC, the development of an efficient PCC design for active power filtering system. In order to extract, for such a system, the filter current and generates the switching signals of SAPF, the modified predictive current controller is considered here as an appropriate technique [20, 21].

The goal of the paper is to enhance the dynamic performance of the SAPF by cooperatively using a STF based PQ algorithm with a novel PCC, enhance the system resilience, ensure optimal management of the total active power between the PV system, the electrical network and the non-linear load by integrating the functionalities of the SAPF under different levels of solar irradiation and maintain the DC-link capacitor voltage constant.

Subject of investigations. This paper describes how an operation of a small scale PV system connected to the low voltage distribution system, and NL can be achieved, the investigation aims to analyze the system's behavior and elucidate the advantages of employing various control algorithms. These proposed algorithms are designed to ensure a unity PF for the utility grid while prioritizing high convergence speed and robustness against load power fluctuations across different levels of solar irradiation affecting the PV modules.

Topologies of an SAPF fed via PV system. The power circuit of the suggested topology of three-phase grid-connected PV and active power filter system can be viewed in Fig. 1. It is designed firstly to inject the real power generated by the PV system to the load on whole days [3]. This topology includes PV panels, a DC-DC boost converter, and a three-phase VSI linked to the low voltage grid via a link inductor. In addition, there's three-phase full bridge rectifier followed by a series resistor and inductor, in parallel with capacitor, which creating NL. The objectives that have been mainly focused in the proposed work are as follows:

1. To effectively demonstrate the multifunctional system's behavior across diverse operating modes and showcase its resilience under challenging conditions.
2. To maintain constant DC-link capacitor voltage of the SAPF under solar irradiance change.
3. To enhance the dynamics performance of SAPF by using STF based PQ algorithm and PCC.
4. To ensure the complete integration of the functionalities of SAPF to compensate the reactive power, suppress the harmonic currents and inject the surplus of active power in the utility grid.

PV array model and its MPPT controller. The combination of numerous PV cells arranged in series and parallel configurations forms a PV generator. Several articles in the literature extensively cover the modeling of these modules [9–11]. The prevalent adoption of a single diode model is attributed to its consistently favorable outcomes. Here, we use the single-diode model to describe the characteristics of PV cells (Fig. 2).

Figure 2 depicts the equivalent circuit of a solitary solar cell, featuring a single diode VD, a parallel resistor R_p, a series resistor R_s, and via Kirchhoff's current law, the output current of the solar PV cell can be expressed as [9]:

$$I_{pv} = I_{ph} - I_d - I_{R_p}; \quad (1)$$

$$I_{pv} = I_{ph} - I_0\left[\exp\left(A\left(V_{pv} + R_s I_{pv}\right)\right) - 1\right] - \frac{V_{pv} - R_s I_{pv}}{R_p}; \quad (2)$$

where I_{ph} is the solar-generated current; I_{pv} is the output current; I_d is the diode current; V_{pv} is the output voltage; I_0 is the diode reverse saturation current; A is the ideality factor of the diode ($1<A<2$).

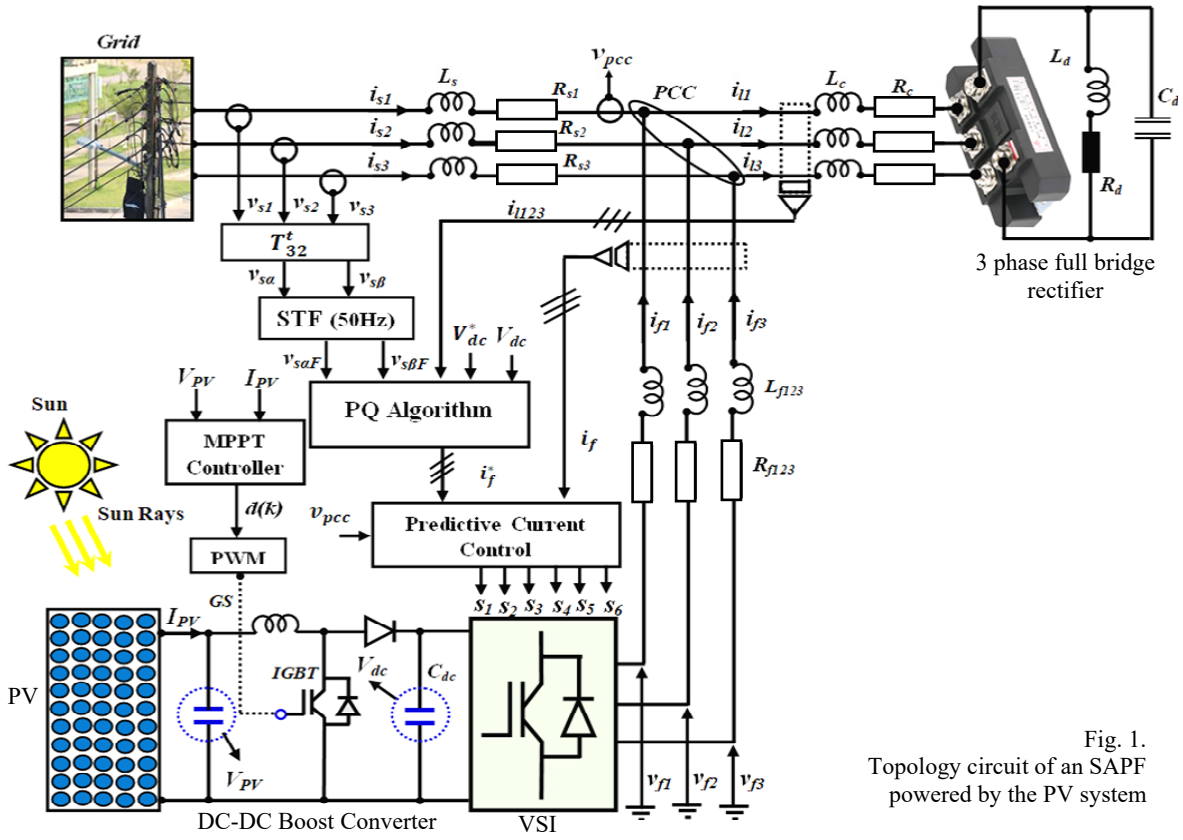

Fig. 1. Topology circuit of an SAPF powered by the PV system

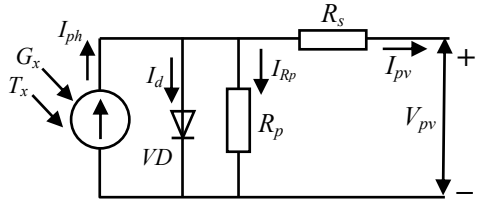

Fig. 2. Equivalent circuit of PV panel

Figure 3 shows the generated outputs characteristics of PV module at T = 25 °C and diverse irradiance. To generate the specified voltage from the simulated model, 120 cells connected in series are required. This system achieves the desired voltage level by applying a gain on the cell voltage equal to the number of sum cells.

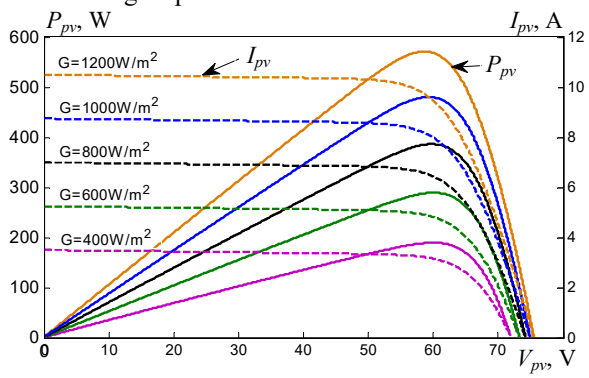

Fig. 3. Characteristic curves $P_{pv} = f(V_{pv})$ and $I_{pv} = f(V_{pv})$ of the PV module

The voltage is determined by ensuring that the PV array operates at its maximum power point (MPP). The P&O algorithm stands out as the most widely adopted MPPT technique, which is used in this work, due to its simplicity and easy implementation. It is based on tracking the MPP by comparing power at different samples times and by periodically perturbing voltage [12]. The working principle of the P&O algorithm is shown in Fig. 4.

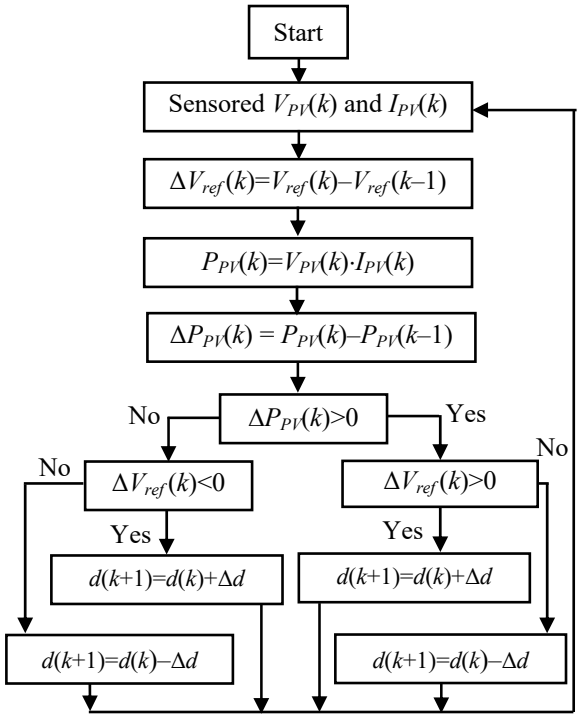

Fig. 4. Flow chart of the P&O algorithm

When PV power P_{PV} and PV voltage V_{PV} increase, the perturbation step size Δd is added to the duty cycle, thus $d(k+1)$ is the next duty cycle value of perturbation, which forces the operating point to move towards the MPP and vice versa. Then, when power P_{PV} increases and V_{PV} decreases, the Δd will be subtracted for the next cycle of perturbation and vice versa. The process is repeated periodically until the MPP is reached. Once the MPP is located by extracting the optimum duty ratio of the boost converter $d(k)$.

The adjustment of the duty ratio for the boost converter is achieved by manipulating the IGBT switches. Gating signals for these IGBT switches are generated by a high carrier frequency pulse-width modulator block, operating at a frequency of 15 kHz (Fig. 5).

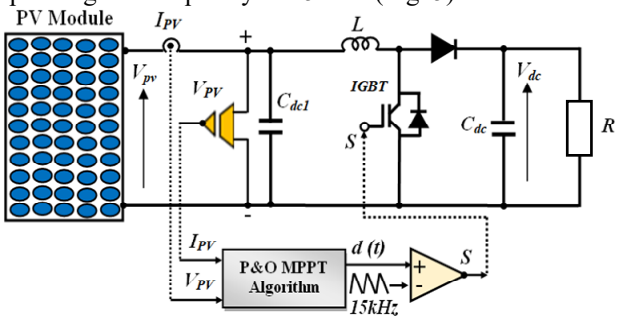

Fig. 5. Scheme control of the PV with DC-DC boost converter

The DC-DC boost converter is driven by the pulse-width modulator's control input $S(t)$. Its operating principle can be expressed by duty cycle D and switching period T_s as follows:

$$S(t)=\begin{cases}0, & 0\le t\le DT_s;\\ 1, & DT_s\le t\le T_s;\end{cases} \quad (3) \qquad V_{dc}=\frac{V_{pv}}{1-D}. \quad (4)$$

Dependent on the switching duty cycle and input voltage V_{pv}, when the IGBT is open, the input capacitor C_{dc1} is charged via the PV panel as per the input voltage, when the IGBT switches ON, current charges up through L, when the IGBT switches back OFF, an opposing voltage is generated and released, the inductor now acts as a voltage source in series with the supply voltage, the output voltage V_{dc} is now charged up to a higher voltage than before, therefore stepping up the voltage.

Indenting the reference harmonics currents. The PQ algorithm is based on a set of instantaneous power defined in the time domain, where the three-phase supply voltages (v_{s1}, v_{s2}, v_{s3}) and currents load (i_{l1}, i_{l2}, i_{l3}) are transformed using the Clarke transformation (α-β) [13], which are written as:

$$\begin{bmatrix}v_{s\alpha}\\ v_{s\beta}\end{bmatrix}=T_{32}^{t}\cdot\begin{bmatrix}v_{s1}\\ v_{s2}\\ v_3\end{bmatrix}=\sqrt{\frac{2}{3}}\begin{bmatrix}\frac{1}{\sqrt{2}} & \frac{1}{\sqrt{2}} & \frac{1}{\sqrt{2}}\\ 1 & \frac{1}{2} & -\frac{1}{2}\\ 0 & \frac{\sqrt{3}}{2} & \frac{\sqrt{3}}{2}\end{bmatrix}\times\begin{bmatrix}v_{s1}\\ v_{s2}\\ v_3\end{bmatrix}; \quad (5)$$

$$\begin{bmatrix}i_{l\alpha}\\ i_{l\beta}\end{bmatrix}=T_{32}^{t}\cdot\begin{bmatrix}i_{l1}\\ i_{l2}\\ i_{l3}\end{bmatrix}=\sqrt{\frac{2}{3}}\begin{bmatrix}\frac{1}{\sqrt{2}} & \frac{1}{\sqrt{2}} & \frac{1}{\sqrt{2}}\\ 1 & \frac{1}{2} & -\frac{1}{2}\\ 0 & \frac{\sqrt{3}}{2} & \frac{\sqrt{3}}{2}\end{bmatrix}\times\begin{bmatrix}i_{l1}\\ i_{l2}\\ i_{l3}\end{bmatrix}. \quad (6)$$

In scenarios where the sources voltage are distorted and unbalanced, the performance of the PQ algorithm is degraded [13], for this a STF is involved and introduced to accurately cleaning the source voltage from these disturbances on the (α-β) axis. This new filter, initially developed in [14, 15] is designed to extract the fundamental component of source voltage amidst distorted and unbalanced conditions. The transfer function of the STF is obtained in the (α-β) axis, it can be expressed as:

$$H(s)=\frac{v_{s\alpha\beta F}}{v_{s\alpha\beta}}=K\frac{s+j\omega_c}{s^2+\omega_c^2}. \quad (7)$$

The value of K is chosen via the frequency response of the STF (Fig. 6,*a*,*b*), when we plot the 3D Bode diagram of the STF for the gain and the phase. It can be noticed that at $\omega_c = 2\pi f_c$ (f_c = 50 Hz) and K=20, the phase angle is equal to 0, and gain is equal 0. This feature allowed us to judge that the fundamental components of the grid voltage are correctly extracted.

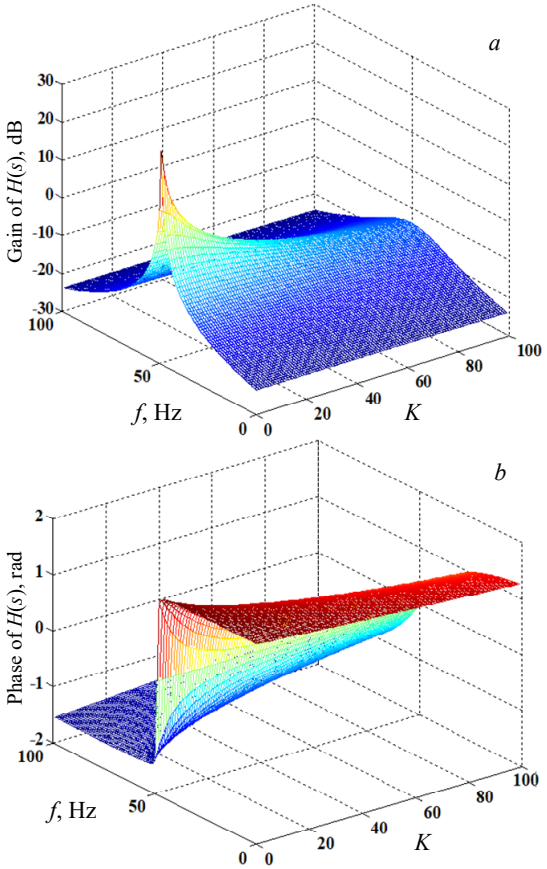

Fig. 6. Frequency response of the STF: gain (*a*) and phase (*b*) of the $H(s)$ for the fundamental

The fundamental of the grid voltage on the (α-β) axis are extracted through (8), (9):

$$v_{s\alpha F}=\frac{20(s+20)}{(s+20)^2+\omega_c^2}v_{s\alpha}(s)-\frac{20\omega_c}{(s+20)^2+\omega_c^2}v_{s\beta}(s); \quad (8)$$

$$v_{s\beta F}=\frac{20\cdot 20\omega_c}{(s+20)^2+\omega_c^2}v_{s\alpha}(s)+\frac{20(s+20)}{(s+20)^2+\omega_c^2}v_{s\beta}(s). \quad (9)$$

Then, the active and reactive instantaneous powers «p» and «q» are given in matrix form:

$$\begin{bmatrix}p\\ q\end{bmatrix}=\begin{bmatrix}v_{s\alpha F} & v_{s\beta F} & 0\\ -v_{s\beta F} & v_{s\alpha F} & 0\\ 0 & 0 & v_0\end{bmatrix}\times\begin{bmatrix}i_{l\alpha}\\ i_{l\beta}\end{bmatrix}. \quad (10)$$

The currents reference in (α-β) axis is obtained as:

$$\begin{bmatrix} i_{h\alpha}^{*} \\ i_{h\beta}^{*} \end{bmatrix} = \frac{1}{v_{s\alpha F}^{2} + v_{s\beta F}^{2}} \begin{bmatrix} v_{s\alpha F} & -v_{s\beta F} \\ v_{s\beta F} & v_{s\alpha F} \end{bmatrix} \times \begin{bmatrix} \tilde{p} \\ q \end{bmatrix}. \quad (11)$$

The three phase reference current of the SAPF can be obtained by applying the inverse Clarke transformation to the stationary reference currents as:

$$\begin{bmatrix} i_{h1}^{*} \\ i_{h2}^{*} \\ i_{h3}^{*} \end{bmatrix} = \sqrt{\frac{2}{3}} \times \begin{bmatrix} 1 & 0 \\ -1/2 & \sqrt{3}/2 \\ -1/2 & -\sqrt{3}/2 \end{bmatrix} \times \begin{bmatrix} i_{h\alpha}^{*} \\ i_{h\beta}^{*} \end{bmatrix}. \quad (12)$$

The three phase reference current of the active power filter can be obtained by applying the inverse Clarke transformation to the stationary reference currents as illustrated by (7).

The required active component I_c, essential for compensating switching losses, is derived from the DC voltage controller. The main task is assigned to the PI controller to maintain the DC-link voltage V_{dc} fixed and ensure the reduced of fluctuation voltage under step change of irradiance solar and sudden change of NL. Furth more the PI regulator provides good performance and high robustness in controlling the system. Voltage control loop diagram can be seen in Fig. 7. It delivered the active component i_c necessary to cover also the switching losses. The final reference harmonic is given as:

$$\begin{bmatrix} i_{f1}^{*} \\ i_{f2}^{*} \\ i_{f3}^{*} \end{bmatrix} = \begin{bmatrix} i_{h1}^{*} \\ i_{h2}^{*} \\ i_{h3}^{*} \end{bmatrix} - \begin{bmatrix} i_{c1} \\ i_{c2} \\ i_{c3} \end{bmatrix}. \quad (13)$$

A graphical representation of the STF based PQ algorithm for determining the reference current filter is depicted in Fig. 7. The resultant reference current derived from this process will be employed in the PCC block of the SAPF, as detailed in the subsequent section, where the STF based PLL is the modified phase looked loop and explained in [16].

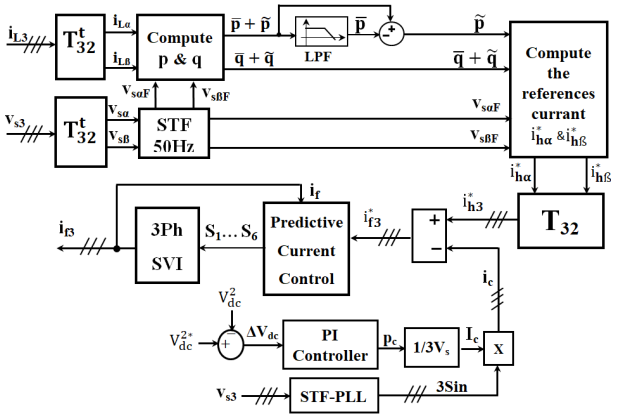

Fig. 7. Diagram of STF based PQ algorithm

Current loop regulation of SAPF using a new PCC. This section concentrates on developing a point of common connection strategy for PV systems feeding SAPFs, while also addressing the generation of reference currents [17, 21]. The initial step involves creating a predictive current model for the SAPF. By deriving the dynamic model of the SAPF from the equivalent single-phase circuit of a three-phase VSI connected to the point of common connection, the strategy is formulated in (14) and as shown in Fig. 8.

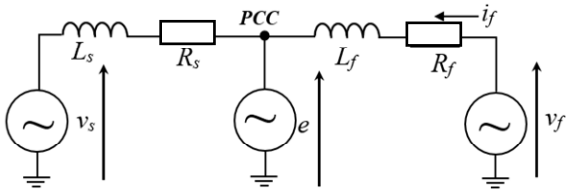

Fig. 8. Simplified scheme of an SAPF

$$\frac{\mathrm{d}i_f}{\mathrm{d}t} + \frac{R_f}{L_f} i_f = \frac{e - v_f}{L_f}, \quad (14)$$

where e is the mains phase voltage at the point of common connection; i_f is the pertinent phase current drawn by the SAPF; v_f is the averaged value of SAPF leg voltage; R_f and L_f are the resistance and the inductance of AC filter inductors.

$$i_f(k+1) = i_f(k) e^{T_s(R_f/L_f)} + \left(E(k) - V_f(k)\right) \cdot \left(\frac{1 - e^{T_s/\tau}}{R_f} \right). \quad (15)$$

Introducing a and b parameters as:

$$a = e^{-T_s(R_f/L_f)} \approx 1 - \frac{R_f}{L_f} T_s;$$

$$b = \frac{1 - e^{-(T_s/\tau)}}{R_f} \approx \frac{1 - 1 + \left(\frac{R_f}{L_f} T_s \right)}{R_f} \approx \frac{T_s}{L_f},$$

where the coefficients a, b are approximated by a Taylor series. The time constant of the output stage of the SAPF is denoted as $\tau = L_f/R_f$.

The SAPF current at time instants k and k+1 is denoted by $i_f(k)$ and $i_f(k+1)$, respectively. The SAPF behavior may be then rewritten as:

$$i_f(k+1) = i_f(k) \cdot a + \left(E(k) - V_f(k)\right) \cdot b. \quad (16)$$

The discrete SAPF model for the sample period between the time instances k+1 and k+2 can be rewritten from (16) in order to design two-steps ahead PCC, as:

$$i_f(k+2) = i_f(k+1) \cdot a + \left(E(k+1) - V_f(k+1)\right) \cdot b. \quad (17)$$

It is remarked that point of common connection voltage is predictable to exhibit a quite sinusoidal waveform, for its prediction, a simple linear extrapolation algorithm was used according to:

$$E(k+1) = 2E(k) - E(k-1). \quad (18)$$

The aim of this PCC is to calculate for the next sampling period T_s between the time instances k+1 and k+2 such an SAPF voltage reference $V_f = V_i$ (i = a, b, c), which is the current error at the time instant k+2 is omitted as shown in Fig. 9.

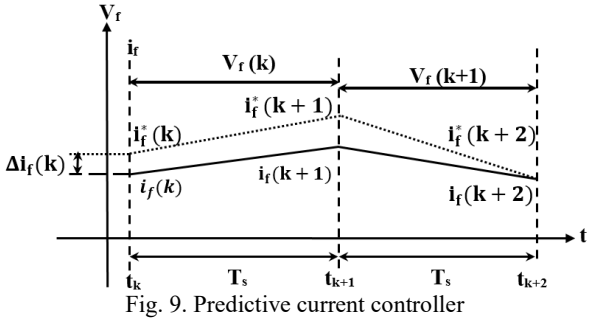

Fig. 9. Predictive current controller

For the purposes of controlling the current error at the sampling period between the time instants k+1 and k+2 can be introduced as:

$$\Delta i_f(k+2) = i_f^*(k+2) - i_f(k+2), \quad (19)$$

where:

$$\Delta i_f(k+2) \cong 0. \quad (20)$$

The reference SAPF average voltage to eliminate current error at the time instant k+2, can then be given from (16) – (18) as:

$$V_f(k+1) = E(k+1) - \frac{1}{b}\left[i_f^*(k+2) - i_f(k+1)a\right]. \quad (21)$$

In applications of the SAPF, current references typically involve the 5th and 7th harmonics, resulting in a complex prediction of the current reference. To overcome this challenge, a polynomial extrapolation technique is suggested for generating current references during transient conditions. Typically, a second-order two-ahead extrapolation method utilizes values from previous sampling instants to estimate the current reference value at time instant k+2

$$i_f^*(k+2) = a_0 i_f^*(k) + a_1 i_f^*(k-1) + a_2 i_f^*(k-2) + \ldots + \ldots + a_n i_f^*(k-n), \quad (22)$$

where a_i (i = 0...n) are the polynomial coefficients to be calculated. There are 9 coefficients to be determined if a compensation of 5th, 7th and 11th harmonics is wanted. Those parameters have been chosen using a genetic algorithm optimization (GAO) based on the minimization of the subsequent fitness function given as:

$$\Delta i_f = \int \left| i_f^*(k) - i_f(k) \right|, \quad (23)$$

where $i_f^*(k)$ represents the predicted current reference at time instant k. The search results obtained using the GAO is summarized in Table 1.

Table 1

Reference generation based GAO parameters

h	5th	7th	11th
a_h	5.3695	–0.2398	11.4581
b_h	–7.1420	2.7384	18.2503
c_h	2.5985	–2.4251	12.8374

Considering the disparity between the modeled filter inductance L_f and its actual value L, the closed-loop transfer function for the current control loop can be described using the following three discrete equations in the z-domain. The first two equations illustrate the behavior of the PCC, while the 3rd equation characterizes the actual plant:

$$V_f(k)z = E(k)\frac{T_s}{L_f} - \left[i_f^*(k)z^2 - -i_f(k+1)\right]; \quad (24)$$

$$i_f(k+1) = E(k)\frac{T_s}{L_f} - V_f(k)L_f + i_f(k); \quad (25)$$

$$V_f(k)z = E(k)z^{-1} - \frac{L_f}{T_s}\left[i_f^*(k) - i_f(k)z^{-1}\right]. \quad (26)$$

From (24) – (26), taking into account the grid voltage as a disturbance, the closed current loop transfer function is:

$$\frac{i_f(z)}{i_f^*(z)} = \frac{\left(L_f / Lz^2\right)}{z^2 + \left(L_f / L^{-1}\right)}. \quad (27)$$

Ignoring the parameters mismatch (i.e L_f/L = 1) in (27) the closed current loop poles must to be moved from the origin to attain better noise rejection. In order to move the current loop closed loop poles from the origin, a new prediction method for the SAPF current at the instant k+1 is:

$$\begin{cases} i_f(k+1) = i_f(k) + i_f^*(k-1) + i_f^*(k) - \Delta i_f(k+1); \\ \Delta i_f(k+1) = i_f(k+1) + i_f^*(k-1); \\ i_f(k+1) = +i_f^*(k+1) + 0.5 i_f^*(k) + 0.5 i_f(k). \end{cases} \quad (28)$$

The block diagram of the overall control structure considering both the voltage, and current control loop is shown in Fig. 10. From this diagram we observe that the SAPF voltages reference values obtained from (21) are forwarded to a space vector modulator functioning in asymmetric [20].

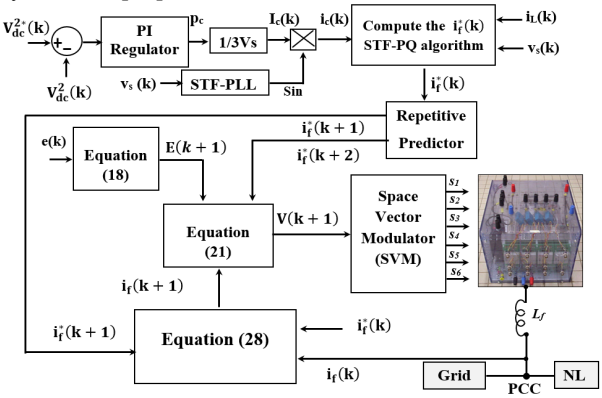

Fig. 10. General control scheme of the SAPF

Simulation results. The efficacy of the proposed system is primarily centered on the grid side. The performance evaluation of the control system is conducted using the STF based PQ algorithm and PCC. Comprehensive testing encompasses all modes of operation, including scenarios involving distorted voltage sources, step changes in solar radiation, and variations in NLs. These assessments are carried out through the MATLAB/Simulink software. Key simulation parameters are outlined in Table 2, and additional details – in Table 3.

Table 2

Physical and electrical characteristics of the PV

Physical characteristic	BP MSX-150
Number of cell in series N_s	72
Number of cell in parallel N_p	1
Standard test conditions	1000 W/m^2, 25 °C
Maximum power P_{max}, W	200
Maximum point voltage V_{mpp}, V	65
Current at maximum point I_{mpp}, A	5.375
Open short circuit voltage V_{oc}, V	26.5

Table 3

System parameters simulated

Parameter	Value
Source resistor R_s, mΩ	20
Source inductance L_s, mH	0.5
DC-Link capacitance C_{dc}, μF	2300
Source frequency f, Hz	50
Source voltage V_s, V	100
Coupling inductance L_f, mH	4.3
Coupling resistor R_f, Ω	1
Load resistance R_d, Ω	290
Load inductance L_d, mH	2
Boost inductance L_b, H	0.04
Load capacitor C_d, μF	1800
K_I	0.1
K	15
T_s, ms	0.005

Testing performance of the proposed system under distorted grid voltage with irradiation G = 900 W/m^2. In this test, the solar irradiation is 900 W/m^2, the waveforms of the first phase of current load (i_{L1}), voltage source (v_{s1}), grid current (i_{s1}), filter current (i_{f1}), DC-link voltage (V_{dc}) and its reference (V^*_{dc}) are illustrate in Fig. 11, the first one, when the grid voltage is sinusoidal and before connected the SAPF into grid, the grid current is distorted with a total harmonic distortion (THD) of 28.27 % and the injected current (i_{f1} = 0), after switching ON the SAPF at t = 0.05 s and when the PQ algorithm is switched OFF, we observe that the grid current remain distorted and in phase opposite with the grid voltage, its THD pass to 25.14 % (Fig. 12,*b*), which mean the filter current contain only the fundamental (Fig. 12,*c*), in this case, there are no harmonics current filtering.

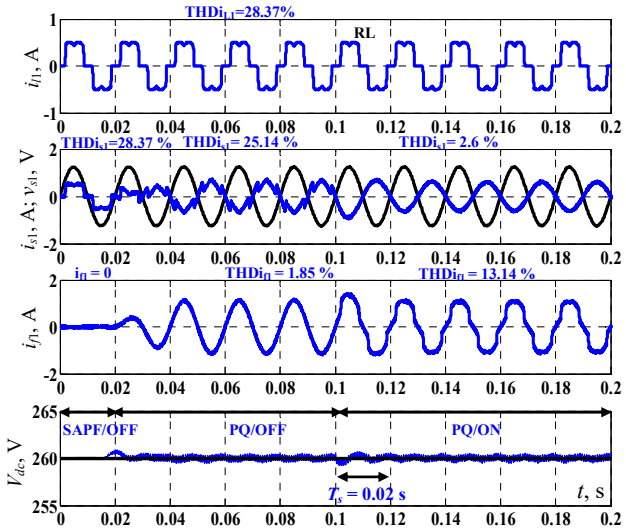

Fig. 11. Performances of the system with ideal grid voltage

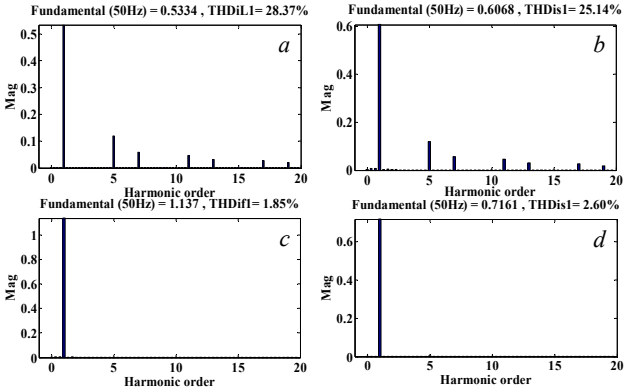

Fig. 12. Harmonic spectrum of i_{L1}, i_{s1} and i_{f1}

After the PQ algorithm is switched ON at 0.1 s, it can be observed that the grid current is sinusoidal with a THD of 2.6 % (Fig. 12,*d*) and the injected current became distorted with a THD of 13.1 % (Table 4), which mean that the SAPF have compensate the harmonic current and the reactive power and inject the fundamental current into grid, which justify the capability of the PCC to manage the dual functionality of the SAPF with the PV system; also we observe that the DC-link voltage track its reference value thanks the PI controller with a less fluctuations, which is dispersed after 0.02 s.

From Fig. 13, when the grid voltage became distorted at the instant 0.2 s with a THD of 9.35 % (Fig. 14,*a*), the grid current is distorted and its THD pass from 2.6 % to 8.96 % (Fig. 14,*c*), we can say that the PQ algorithm is not suitable to generate the reference harmonics current. But after turned ON the STF-PQ algorithm at the instant 0.03 s, the grid current recovers its sinusoidal wave form and noted an enhanced of its THD, it passes from 8.86 % to 2.72 % (Fig. 14,*d*). The detailed results are depicted in Table 4.

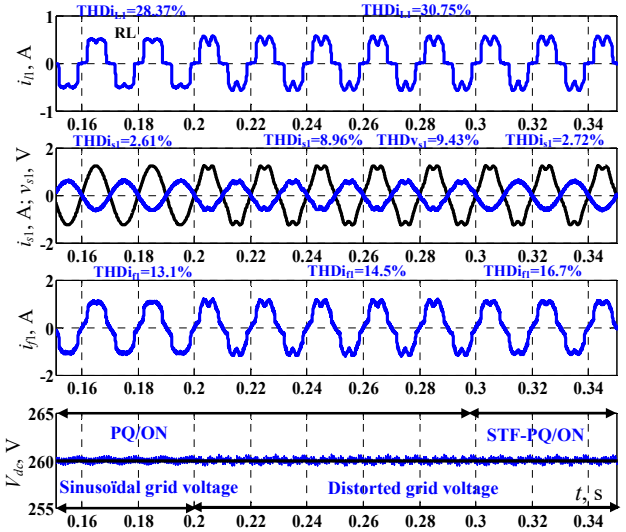

Fig. 13. Performance of the system with distorted grid voltage

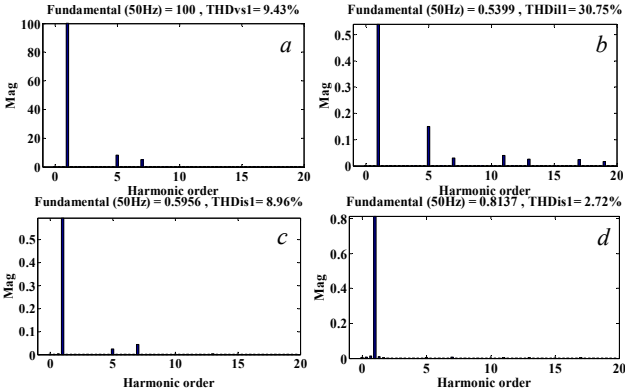

Fig. 14. Harmonic spectrum of v_{s1}, i_{L1} and i_{s1}

The flow of the active power and reactive power is illustrated in Fig. 15, which demonstrate clearly how the system control proposed have mange all the operation modes under distorted grid voltage.

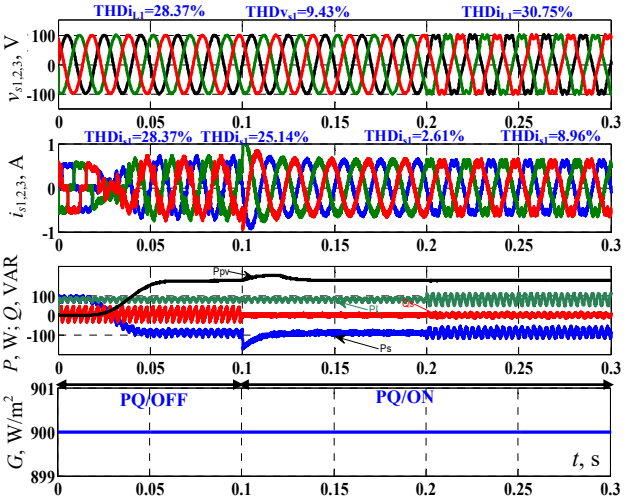

Fig. 15. Behavior the grid, PV and NL under distorted grid voltage

It can be seen that active power of grid P_s is negative after turned ON the SAPF, which mean that the active power P_{pv} generated by the PV is injected into the grid after satisfying the need of active power P_L of the NL; also reactive power of the grid is null, which means that the unity PF is reached. This major performance has been degraded when the grid voltage is distorted by the appearance of fluctuations of power system; values of the power are recapped in Table 4.

Table 4

Performance of the proposed system under distorted voltage

G, W/m^2	900 W/m^2 [0 – 0.4 s] and R_d, L_d				
V_s, V	Sinusoidal [0 – 0.1 s]		Distorted THD = 9.43 %		
State/SAPF	SAPF/OFF	SAPF/ON [0.1 – 0.3 s] and PF=0.989			
STF, PQ	PQ/OFF	PQ/OFF	PQ/ON		STF-PQ/ON
THDi_{s1}, %	28.14	25.14	2.6	8.8	2.72
THDi_{f1}, %	0	1.85	13.1	14.5	16.7
P_s, W	80	–95	–95	–89	–95
Q_s, VAR	6	6	0	0	0
P_{ch}, W	80	80	80	82	82
P_{pv}, W	0	175	175	175	176

Testing performance of the system under distorted and unbalanced grid voltage with irradiation 900 W/m^2. At the instant 0.2 s, under solar irradiation of 900 W/m^2 and under grid voltage distorted and unbalanced condition we observe that as the grid current is distorted and in phase with the grid voltage (Fig. 16), which is justified by the harmonic spectrum of the grid current that take the value of 16.7 % (Fig. 17,*a*).

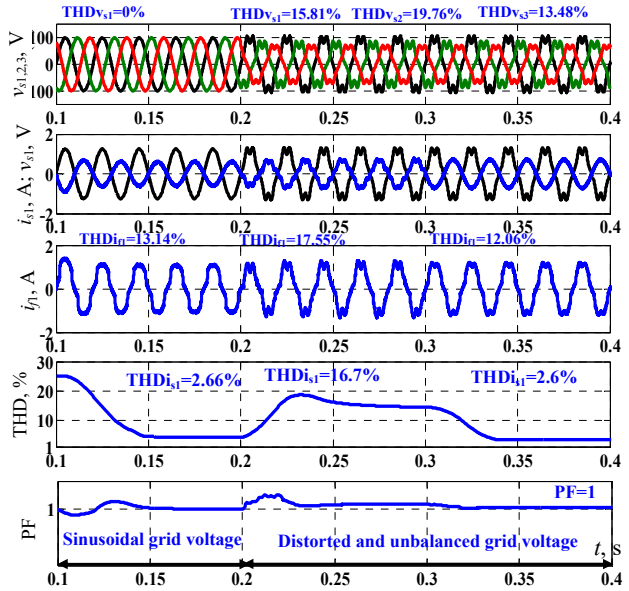

Fig. 16. Performance of the system under distorted unbalanced grid voltage

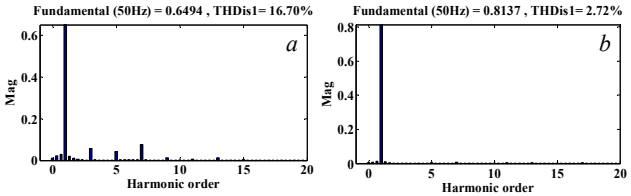

Fig. 17. Harmonic spectrums of i_{s1} without (*a*) and with (*b*) using the STF based PQ algorithm

That means that the PQ algorithm is not efficient in this condition, and after having activated the STF-PQ algorithm at the instant 0.3 s, the grid current recover its sinusoidal wave form, and we can say that the proposed system has become robust to this change. Additionally, the predictive current controller proves its faster response time to quickly generate the switching signal for the VSI of the SAPF. The performances guaranteed by this test have been specified in Table 5.

Table 5

Performance of the system under distorted unbalanced voltage

G, W/m^2	900 W/m^2 [0 – 0.6 s]			
V_s, V	Distorted unbalanced THD=15.81 % [0.2 – 0.6 s]			
State/SAPF	SAPF/ON [0.1 – 0.3 s] and PF = 1			
STF, PQ	PQ/OFF	PQ/ON		STF-PQ/ON
THDi_{s1}, %	25.14	2.72	16.7	2.6
THDi_{f1}, %	1.85	13.1	17.5	12.06
P_s, W	–95	–95	–89	–88.9
Q_s, VAR	6	0	0	0
P_{ch}, W	80	80	82	60
P_{pv}, W	175	175	175	175

Testing performance of the proposed system under NL change. In this test (Fig. 18, 19), the dynamic performance of proposed system is investigated under solar irradiation G = 900 W/m^2 and under step change of NL, where a capacitor of 15 µF is inserted in parallel with the inductance load at the instant of 0.4 s and disconnected at the instant 0.45 s, we notice that the value of the grid current is decreased to 0.016 A (Fig. 19,*a*), and the filter current provided by the SAPF is similar to the NL current, which mean that the NL is supplied by the PV generator and all the active power generated is provide to the NL.

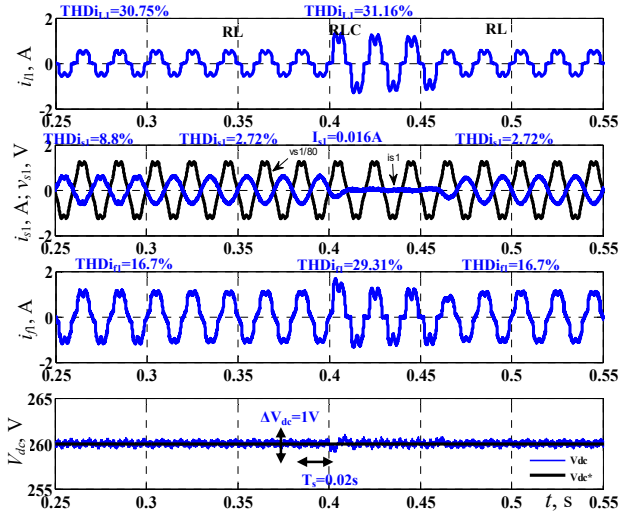

Fig. 18. Waveforms of i_{L1}, $v_{s1,}$ i_{s1}, i_{f1} and V_{dc} under NL change

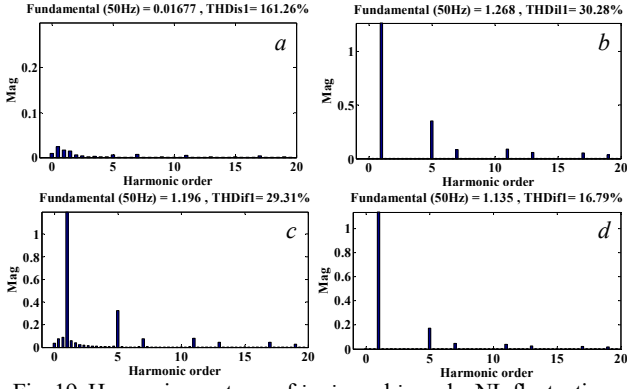

Fig. 19. Harmonic spectrum of i_{s1}, i_{L1} and i_{f1} under NL fluctuations

In this case the grid does not provide any active power, also, when we disbranched the capacitor load at the instant of 0.45 s. The an extra sinusoidal current is appeared into

grid with a THD of 2.72 %, and through these very satisfactory results we confirm the good operation of the proposed system in this case, and the PI controller with PCC reached its main role to manage the flow of active power between the grid, the NL and PV generator.

Testing performance test under gradual change of solar irradiation and NL change. From Fig. 20, when we proceed a step change of solar irradiation from G = 900 W/m^2 to 200W/m^2 (between the instant time of 0.6 s and 0.85 s), when the STF-PQ/ON and under distorted grid voltage (THDv_{s1} = 9.45 %), we remark that the source current drops to 0 after one period (I_{s1} = 0.00667 A) as depicted by the harmonics spectrum in Fig. 21,*a*, indicating that all the active power generated by the PV array is entirely consumed by the NL, and grid no provide any active power as can be seen in Fig. 22. For the second test, under G = 200 W/m^2 and when we increasing the NL current by decreasing the value of the value of NL between the instants (0.7 s – 0.8 s), we observe that grid current is sinusoidal and in phase with the grid voltage which confirm that the PF is unity, also proved the capability and the robustness of the controllers to precisely track their reference current. And by reading the value of spectrum of the grid current in this test, it can be noticed that the THD take the value of 2.66 % as depicted in Fig. 21,*b*.

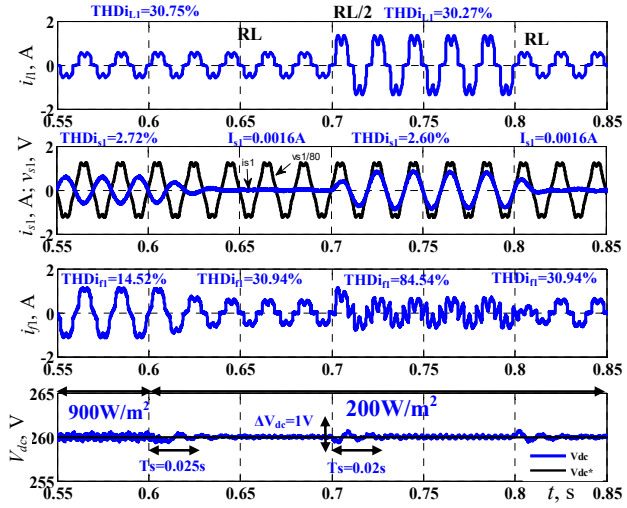

Fig. 20. Performance under step change in solar irradiation and NL

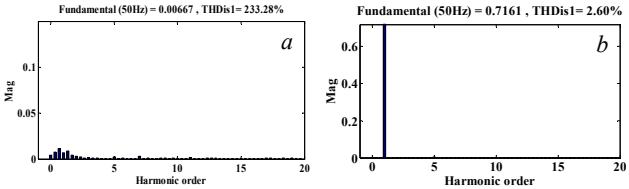

Fig. 21. Harmonic spectrum of i_{s1} and i_{f1} under step change of solar irradiation

Additionally, Fig. 22 illustrates that both active and reactive power sources become null, indicating that the grid does not supply any power to the load. These findings provide insights into the system's robust performance under varying irradiation conditions, showcasing its ability to adapt and maintain stable operation, and all the obtained results of this sever test are presented in Table 6.

Table 6

Performance of the system under distorted unbalanced voltage

G, W/m^2	900	200	
Load type	(R_d+L_d+C_d)	(R_d+L_d)	(R_d+L_d)/2
t, s	[0.4–0.45]	[0.6–0.7]	[0.7–0.8]
THDi_{s1}, %	0 (I_s≈0)	0 (I_s=0)	2.66 %, PF=1
THDi_{f1}, %	29.31	30.94	84.54
THDi_{L1}, %	31.16	30.75 %	30.75
P_s, W	0.05	0	128
Q_s, VAR	0.05	0	0
P_{ch}, W	175	82	192
P_{pv}, W	175	82	82

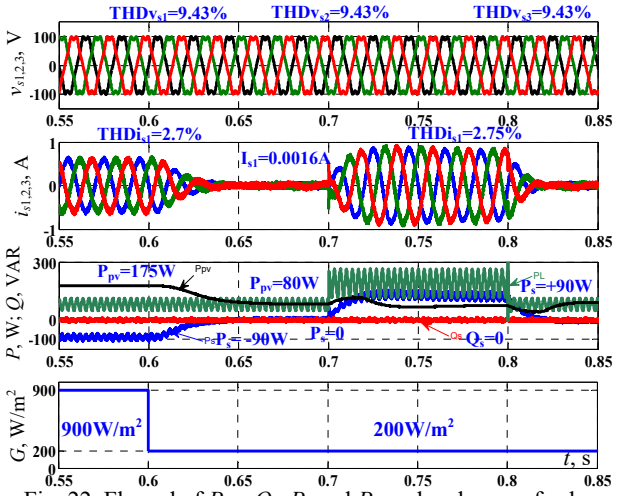

Fig. 22. Flowed of P_{PV}, Q_s, P_s and P_L under change of solar irradiation and NL

Testing performance of the proposed system under fluctuations of solar irradiation. At the instant 0.9 s, when solar radiation increased from 200 W/m² to 900 W/m², we noticed from Fig. 23 that the SAPF is capable of cleaning the grid from the current harmonics generated by the NL and the grid current will be in opposite phase with the grid voltage, which means that the unity PF is reached in this operation condition. In addition, the efficiency the SAPF's algorithm control is confirmed by injecting filter current to compensate the harmonic load current and injecting the fundamental current in the grid, this results is justified by reading the THD of the grid current, it passes from 28.14 % to 3.51 % after switching ON the SAPF as depicted in Fig. 22, then the IEEE-519 standard is satisfactory.

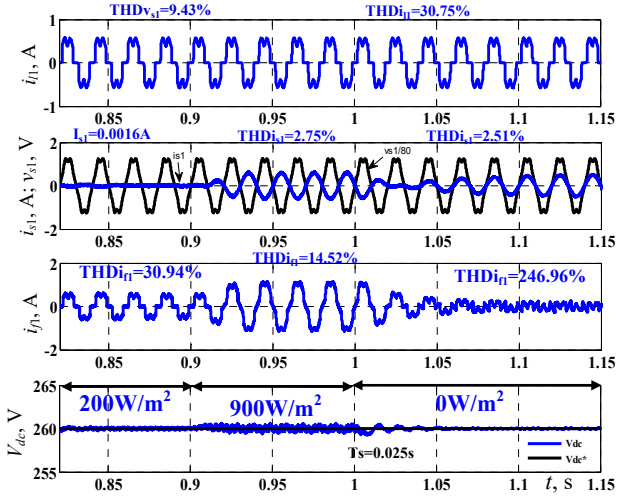

Fig. 23. Behavior of the system when the solar irradiation change (200 / 0 / 900) W/m^2

Its can be observed that the reactive source is drawn to 0, which justify the good behavior of the proposed system to compensate the reactive power generated by the NL. Also the active power is 90 W, which illustrate that the SAPF inject into grid the surplus of the active power provided by the PV system and the NL is fed from the PV system.

The third test is carried out at the instant 1 s, when the solar irradiation is drawn to G=0, it can be observed from Fig. 23 that the grid current is become positive and in phase with the grid voltage, and kept its sinusoidal waveform and its THD pass to 2.52 % (Fig. 24,*a*), the filter current is high distorted and contain only the reactive fundamental and harmonic current (its THD pass from 14.52 % to 246.9 %), then we can say the unity PF is obtained in this condition and the harmonic current are suppression.

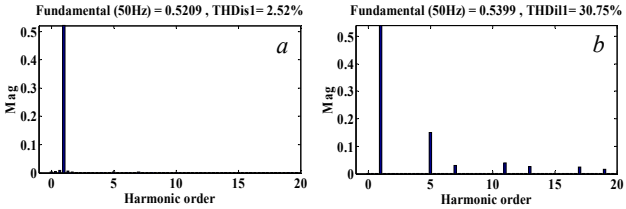

Fig. 24. Harmonic spectrum of i_{s1} and i_{L1}

On the other hand, from Fig. 25, it can be remarked that the active power source become positive, which signify that the PV system no provide any power and the NL is supplied by the grid (P_s = 90 W). We can prove, through these performance tests, that the control algorithms applied to the proposed system have fulfilled their main roles, for which they were designed, under different solar radiations, different types of loads and under non-optimal grid voltage. The results of this performance test are given in Table 7.

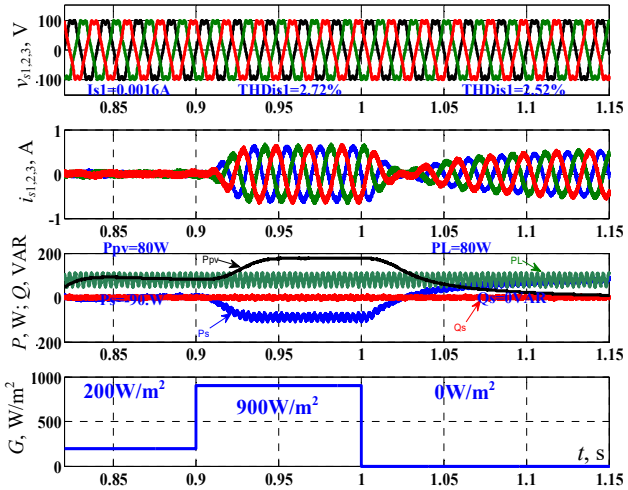

Fig. 25. Flowed of the P_{pv}, Q_s, P_s and P_L under solar irradiation changes

Table 7

Performance of the system under distorted unbalanced voltage

G, W/m^2	0 W/m^2 [1–1.2 s] STF-PQ	900 W/m^2 [1.2–1.3 s] STF-PQ
THDi_{L1}, %	30.75	30.75
THDi_{s1}, %	2.52 % and PF=1	2.72 % and PF=1
THDi_{f1}, %	246.96	14.52
P_s, W	81	–90
Q_s, VAR	0	0
P_{ch}, W	81	81
P_{pv}, W	0	175

Conclusions. In this work, a dual functionality of a double stage grid connected PV system has been performed, analyzed and examined. The majors' tasks of the proposed system have been realized desired target throughout inserting a series active filter concept with injection of the surplus active power into the grid during periods of low overall demand.

From electrical network side, a novel PCC based on discrete-time model for controlling source voltage inverter of the SAPF has been developed. Moreover, modified PQ algorithm, which based on the STF was used for accurately extracting the reference filter currents required for PCC, of which turn, facilitates the generation of the SAPF's switching signals.

From the PV generator side, a P&O based MPPT algorithm has been used to extract MPP generated by the PV array which governs the duty cycle of the DC-DC boost converter. To prove the efficiency of the proposed framework, multiples comprehensive testing has been undergone considering the variations in nonlinear loads and solar radiation fluctuations.

Simulated results highlight superior performance in both transient and stable states, affirming the robustness and effectiveness of the proposed controllers, and thanks to them, we achieved impressive results, by reading the power supply current distortion index, which reduced the THD to less than 5 % according to IEEE-519 standard, which indicates that the proposed system is robust, homogeneous, and performs its assigned role with distinction.

Conflict of interest. The authors declare that they have no conflicts of interest.

REFERENCES

1. El-Habrouk M., Darwish M.K., Mehta P. Active power filters: A review. *IEE Proceedings - Electric Power Applications*, 2000, vol. 147, no. 5, pp. 403-413. doi: https://doi.org/10.1049/ip-epa:20000522.

2. Hamouda N., Babes B., Kahla S., Hamouda C. Uwe R. An optimized FO-PID controller and predictive current control of the APF connected AWPS for power quality improvement. *Przeglad Elektrotechniczny*, 2023, vol. 99, no. 5, pp. 102-107. doi: https://doi.org/10.15199/48.2023.05.19.

3. Dash D.K., Sadhu P.K. A Review on the Use of Active Power Filter for Grid-Connected Renewable Energy Conversion Systems. *Processes*, 2023, vol. 11, no. 5, art. no. 1467. doi: https://doi.org/10.3390/pr11051467.

4. Patidar R.D., Singh S.P., Khatod D.K. Single-phase single-stage grid-interactive photovoltaic system with active filter functions. *IEEE PES General Meeting*, 2010, pp. 1-7. doi: https://doi.org/10.1109/PES.2010.5588185.

5. Shah P.K., Kotwal C.D., Giri A.K., Chitti Babu B. Study of multi-objective photovoltaic grid connected system using SOGI-FLL and NL-SOGI-FLL-APF based DQ hysteresis method. *Electrical Engineering*, 2023, vol. 105, no. 5, pp. 2735-2749. doi: https://doi.org/10.1007/s00202-023-01817-3.

6. Bourouis B., Djeghloud H., Benalla H. Energy efficiency of a 3-level shunt active power filter powered by a fuel-cell / battery DC bus with regulated duty cycles. *Electrical Engineering & Electromechanics*, 2021, no. 5, pp. 30-38. doi: https://doi.org/10.20998/2074-272X.2021.5.05.

7. Ouchen S., Betka A., Abdeddaim S., Menadi A. Fuzzy-predictive direct power control implementation of a grid connected photovoltaic system, associated with an active power filter. *Energy Conversion and Management*, 2016, vol. 122, pp. 515-525. doi: https://doi.org/10.1016/j.enconman.2016.06.018.

8. Reisi A.R., Moradi M.H., Showkati H. Combined photovoltaic and unified power quality controller to improve power quality. *Solar Energy*, 2013, vol. 88, pp. 154-162. doi: https://doi.org/10.1016/j.solener.2012.11.024.

9. Nordin A.H.M., Omar A.M. Modeling and simulation of Photovoltaic (PV) array and maximum power point tracker (MPPT) for grid-connected PV system. *2011 3rd International Symposium & Exhibition in Sustainable Energy & Environment (ISESEE)*, 2011, pp. 114-119. doi: https://doi.org/10.1109/ISESEE.2011.5977080.
10. Zerzouri N., Ben Si Ali N., Benalia N. A maximum power point tracking of a photovoltaic system connected to a three-phase grid using a variable step size perturb and observe algorithm. *Electrical Engineering & Electromechanics*, 2023, no. 5, pp. 37-46. doi: https://doi.org/10.20998/2074-272X.2023.5.06.
11. Elgendy M.A., Zahawi B., Atkinson D.J. Assessment of Perturb and Observe MPPT Algorithm Implementation Techniques for PV Pumping Applications. *IEEE Transactions on Sustainable Energy*, 2012, vol. 3, no. 1, pp. 21-33. doi: https://doi.org/10.1109/TSTE.2011.2168245.
12. Babes B., Albalawi F., Hamouda N., Kahla S., Ghoneim S.S.M. Fractional-Fuzzy PID Control Approach of Photovoltaic-Wire Feeder System (PV-WFS): Simulation and HIL-Based Experimental Investigation. *IEEE Access*, 2021, vol. 9, pp. 159933-159954. doi: https://doi.org/10.1109/ACCESS.2021.3129608.
13. Salmeron P., Herrera R.S. Distorted and Unbalanced Systems Compensation Within Instantaneous Reactive Power Framework. *IEEE Transactions on Power Delivery*, 2006, vol. 21, no. 3, pp. 1655-1662. doi: https://doi.org/10.1109/TPWRD.2006.874115.
14. Abdusalam M., Poure P., Saadate S. Study and experimental validation of harmonic isolation based on High Selectivity Filter for three-phase active filter. *2008 IEEE International Symposium on Industrial Electronics*, 2008, pp. 166-171. doi: https://doi.org/10.1109/ISIE.2008.4676991.
15. Biricik S., Redif S., Khadem S.K., Basu M. Improved harmonic suppression efficiency of single-phase APFs in distorted distribution systems. *International Journal of Electronics*, 2016, vol. 103, no. 2, pp. 232-246. doi: https://doi.org/10.1080/00207217.2015.1036318.
16. Chemidi A., Benhabib M.C., Bourouis M.A. Performance improvement of shunt active power filter based on indirect control with a new robust phase-locked loop. *Electrical Engineering & Electromechanics*, 2022, no. 4, pp. 51-56. doi: https://doi.org/10.20998/2074-272X.2022.4.07.
17. Rodriguez J., Pontt J., Silva C.A., Correa P., Lezana P., Cortes P., Ammann U. Predictive Current Control of a Voltage Source Inverter. *IEEE Transactions on Industrial Electronics*, 2007, vol. 54, no. 1, pp. 495-503. doi: https://doi.org/10.1109/TIE.2006.888802.
18. Boukezata B., Gaubert J.-P., Chaoui A., Hachemi M. Predictive current control in multifunctional grid connected inverter interfaced by PV system. *Solar Energy*, 2016, vol. 139, pp. 130-141. doi: https://doi.org/10.1016/j.solener.2016.09.029.
19. Zine H.K.E., Abed K. Smart current control of the wind energy conversion system based permanent magnet synchronous generator using predictive and hysteresis model. *Electrical Engineering & Electromechanics*, 2024, no. 2, pp. 40-47. doi: https://doi.org/10.20998/2074-272X.2024.2.06.
20. Bouafia A., Gaubert J.-P., Krim F. Predictive Direct Power Control of Three-Phase Pulse Width Modulation (PWM) Rectifier Using Space-Vector Modulation (SVM). *IEEE Transactions on Power Electronics*, 2010, vol. 25, no. 1, pp. 228-236. doi: https://doi.org/10.1109/TPEL.2009.2028731.
21. Hamouda N., Benalla H., Hemsas K., Babes B., Petzoldt J., Ellinger T., Hamouda C. Type-2 fuzzy logic predictive control of a grid connected wind power systems with integrated active power filter capabilities. *Journal of Power Electronics*, 2017, vol. 17, no. 6, pp. 1587-1599. doi: https://doi.org/10.6113/JPE.2017.17.6.1587.

Received 28.03.2024
Accepted 20.05.2024
Published 21.10.2024

Assam Zorig[1]*, Associate Professor,*
Badreddine Babes[2]*, Senior Researcher,*
Noureddine Hamouda[2]*, Senior Researcher,*
Souhil Mouassa[3]*, Professor,*
[1] Department of Electrical Engineering,
Faculty of Technology, Mohamed Boudiaf University, Algeria,
e-mail: assam.zorig@univ-msila.dz
[2] Research Center in Industrial Technologies, Algeria,
e-mail: b.babes@crti.dz; n.hamouda@crti.dz
[3] University of Bouira, Algeria,
e-mail: souhil.mouassa@univ-bouira.dz (Corresponding Author)

How to cite this article:
Zorig A., Hamouda N., Babes B., Mouassa S. Improving the efficiency of a non-ideal grid coupled to a photovoltaic system with a shunt active power filter using a self-tuning filter and a predictive current controller. *Electrical Engineering & Electromechanics*, 2024, no. 6, pp. 33-43. doi: https://doi.org/10.20998/2074-272X.2024.6.05